

Numerov extension of transparent boundary conditions for the Schrödinger equation in one dimension

Curt A. Moyer^{a)}

Department of Physics and Physical Oceanography, UNC Wilmington, Wilmington, North Carolina 28403

(Received 17 April 2003; accepted 22 August 2003)

We describe an algorithm for animating time-dependent quantum wave functions in one dimension with very high accuracy. The algorithm employs the Crank–Nicholson approximation for the time dependence along with a Numerov extension of the discrete transparent boundary conditions described recently by Ehrhardt. We illustrate the power of this approach by simulating the decay of alpha particles from radioactive nuclei and the resonance scattering of electrons in a three-layer GaAs–GaAlAs sandwich. © 2004 American Association of Physics Teachers.
[DOI: 10.1119/1.1619141]

I. INTRODUCTION

Numerical simulations of time-dependent Schrödinger wave functions in one space dimension began in earnest with the computer-generated motion pictures of Goldberg, Shey, and Schwartz,¹ and first emerged as a teaching aid for undergraduate quantum mechanics in the hands of Chen.² All numerical studies since then share with these studies the requirement that the wave function be zero at the end points of the interval. These rigid-wall boundary conditions work well when the quantum state is forever confined, such as the admixture of low-lying states of a potential well. But problems arise in the treatment of scattering problems for which great care must be exercised to avoid spurious reflections of the reflected and transmitted waves at the boundaries. These unwanted reflections restrict the usable portion of the spatial interval used for computation and limit the duration of the scattering event in ways that are artificial. With the advent of transparent boundary conditions,^{3–6} these limitations can be overcome. The use of transparent boundary conditions makes it possible to mimic a spatial domain of infinite extent using boundary conditions at the end points of a finite interval. The discretization of transparent boundary conditions has itself proved problematic, but recently Arnold and Ehrhardt have pioneered a technique that yields the proper discrete transparent boundary conditions.^{7,8} With discrete transparent boundary conditions, there is no need to artificially impose restrictions on space and time: wave packet scattering can be simulated in an interval that includes little more than the target, and the event can be followed as long as desired, at least in principle.

The discrete transparent boundary conditions developed in Refs. 7 and 8 are based on a centered-difference approximation to the second spatial derivative of the evolving wave function. Here we formulate discrete transparent boundary conditions based on the Numerov approximation, which is accurate to fifth order in the spatial step size. The improved spatial accuracy afforded by the Numerov extension comes at a very modest computational cost. Numerical results are presented for simulating alpha decay of a radioactive nucleus, and resonant scattering from a layered semiconductor.

II. THE ALGORITHM

We seek numerical solutions to the time-dependent Schrödinger equation in one space dimension, given the initial

wave function $\psi(x, t_0)$. In natural units, $\hbar = 1$, $m = 1/2$, the system propagator is $\exp(-iHt)$, where $H = -\partial^2/\partial x^2 + V(x)$ is the Hamiltonian operator and the system potential energy $V(x)$ is taken to be time-independent. The wave function obeys the relation $\psi(x, t + \Delta) = \exp(-iH\Delta)\psi(x, t)$; it is this relation that must be discretized in space and time.

A. Crank–Nicholson method

The well-known Crank–Nicholson method⁹ replaces the system propagator with the Cayley form,

$$\exp(-iH\Delta) = \frac{1 - iH\Delta/2}{1 + iH\Delta/2} + O(\Delta^3), \quad (1)$$

which is accurate to second order in the time step Δ . Like the exact propagator, this replacement has the virtue of being unitary, and therefore is norm-preserving and inherently stable. The Crank–Nicholson approximation to the evolution problem is then

$$[1 + iH\Delta/2]\psi(x, t + \Delta) \approx [1 - iH\Delta/2]\psi(x, t). \quad (2)$$

We prefer to rewrite Eq. (2) in terms of a new function $y(x, t) \equiv \psi(x, t + \Delta) + \psi(x, t)$. If we use the definition of H , we find

$$\frac{\partial^2 y}{\partial x^2} - \left[V(x) - i \frac{2}{\Delta} \right] y(x, t) = i \frac{4}{\Delta} \psi(x, t), \quad (3)$$

where $\psi(x, t)$ is known (from the previous step) and $y(x, t)$ is to be found from Eq. (3).

At this point, the usual numerical procedure is to replace the second derivative in Eq. (3) by the centered-difference, $h^2 \partial^2 y / \partial x^2 \approx y(x+h) + y(x-h) - 2y(x)$, and solve the resulting difference equation for y , which is accurate to third order in the space increment h . With just a little more computational effort, however, we can realize results accurate to fifth order in h using the Numerov method, as described below.

B. Space discretization: The Numerov approximation

In terms of the variable x , Eq. (3) has the structure $y''(x) = g(x)y(x) + f(x)$, which lends itself to the Numerov method. Briefly, the idea is to use this equation to evaluate the next order term in a discrete approximation to the second derivative. To facilitate the discussion, we abbreviate $y(x_j$

$=x_0+jh$) as y_j , and similarly for $g(x_j)$ and $f(x_j)$. Then a straightforward Taylor expansion about x_j yields

$$y_{j+1}+y_{j-1}-2y_j=y''(x_j)h^2+\frac{1}{12}y^{(4)}(x_j)h^4+O(h^6), \quad (4)$$

where $y^{(4)}$ is the fourth derivative of y with respect to x . If we truncate Eq. (4) at the first term, we reproduce the familiar centered-difference approximation to the second derivative. To evaluate $y^{(4)}(x_j)$, we note that it is $(gy+f)''|_{x_j}$ and use the usual centered-difference approximation once more to obtain

$$y^{(4)}(x_j)h^2=g_{j+1}y_{j+1}+f_{j+1}+g_{j-1}y_{j-1}+f_{j-1}-2g_jy_j-2f_j+O(h^4). \quad (5)$$

We substitute this result into Eq. (4) to obtain a refined estimate of $y''(x_j)$. We use this result to transform the original equation, which in our notation becomes $y''(x_j)=g_jy_j+f_j$, to a finite difference relation that differs from the original by terms that are of order $O(h^6)$. In terms of the two new functions $d_j\equiv 1-h^2g_j/12$ and $w_j\equiv d_jy_j-h^2f_j/12$, the result takes the very compact form

$$w_{j+1}+w_{j-1}=\left[2+h^2\frac{g_j}{d_j}\right]w_j+h^2\frac{f_j}{d_j}. \quad (6)$$

For comparison, we note that the less accurate centered-difference approximation to the second derivative yields an equation identical to Eq. (6), but with $d_j\equiv 1$ and $w_j\equiv y_j$.

The quantities w_j , y_j , and f_j also depend on the time t , which we discretize as $t_n=t_0+n\Delta$, and track using the notation: $w_j\rightarrow w_j^n\equiv d_jy_j^n-h^2f_j^n/12$. The Crank–Nicholson procedure, Eq. (3), is described by $y_j^n=\psi_j^{n+1}+\psi_j^n$, $g_j=V_j-2i/\Delta$, and $f_j^n=4i\psi_j^n/\Delta$.

Equation (6) is a three-term recursion relation for the unknown w_j . The numerical solution is straightforward if the initial values, say w_0^n and w_1^n , are known, but this information is atypical for evolution problems. More commonly, the wave function can be assumed to vanish at the end points of a sufficiently large interval, corresponding to $w_0^n=w_J^n=0$ for some $J>0$ and all n . Goldberg *et al.* showed how such rigid-wall boundary conditions can be handled numerically.¹ Their technique is to reduce the original three-term recursion relation to a pair of two-term recursions for two new functions e_j and q_j^n by requiring that $w_{j+1}^n=e_jw_j^n+q_j^n$ for all $j=1,2,\dots,J-1$. If we use this relation in Eq. (6), we find

$$e_j+\frac{1}{e_{j-1}}=2+h^2\frac{g_j}{d_j}, \quad (7a)$$

$$q_j^n=\frac{q_{j-1}^n}{e_{j-1}}+h^2\frac{f_j^n}{d_j}. \quad (7b)$$

Equation (7) generates e_j and q_j^n from the initial values e_0 and q_0^n . The two-for-one replacement means that one of these data points may be chosen arbitrarily, while the other is dictated by the boundary conditions. The trick is to recognize that for rigid walls ($w_0^n=0$), we can let $e_0\rightarrow\infty$, thus permitting both e_j and q_j^n to be found immediately from Eq. (7), assuming only that q_0^n is finite. Then, starting with $w_J^n=0$, we can use $w_{j-1}^n=(w_j^n-q_{j-1}^n)/e_{j-1}$ to construct $w_{j-1}^n, w_{j-2}^n, \dots, w_1^n$. As a bonus, we note that for the evo-

lution problem, the e_j need be computed just *once* at the start of the process (by contrast, the q_j^n must be recalculated at each time step n).

The foregoing procedure is the one traditionally followed in animating one-dimensional quantum wave functions. And although the method easily accommodates the improved accuracy afforded by the Numerov scheme, the author is unaware of any simulations that employ this refinement. In any case, the rigid-wall boundary conditions pose unacceptable limitations in scattering problems or other situations (for example, radioactive decay) where the wave function is not inherently confined. With transparent boundary conditions or, more precisely, discrete transparent boundary conditions, these limitations can be completely overcome.

C. Transparent boundary conditions

Transparent boundary conditions enable us to mimic a spatial domain of infinite extent using boundary conditions applied at the end points of a finite interval. In quantum applications, this interval must support the initial wave function, which is required to vanish everywhere in the exterior.¹⁰ The exterior region also is assumed to be force free, so that the potential energy is constant there. The original transparent boundary condition formulation for the Schrödinger equation dates to 1982,³ but only recently has the proper discretization of the results been given,^{7,8} thereby opening the door to the full power of the method. Because this work is not well known or readily accessible to many physicists, we outline in the Appendix the principal ideas and results. The Appendix also establishes corrections to the standard treatment that are necessary when the Numerov scheme is employed.

For our purposes, the basic point is that the boundary condition on the left ($j=0$) takes the form $w_1^n=\alpha w_0^n+\beta^n$, where α and β^n are given in the Appendix. If we compare with $w_1^n=e_0w_0^n+q_0^n$, we find $e_0=\alpha_0$ and $q_0^n=\beta_0^n$ [see Eq. (A15)]:

$$e_0=\alpha_0=a_0\pm\sqrt{a_0^2-1}, \quad (8a)$$

$$q_0^n=\beta_0^n=d_0^*(a_0^*-\alpha_0)\psi_0^n+d_0(a_0-\alpha_0)\sum_{k=1}^n\ell_{n-k+1}\psi_0^k. \quad (8b)$$

Here d_0 and a_0 denote the values at $j=0$ taken by $d_j=1-h^2g_j/12$ and $a_j=1+h^2g_j/2d_j$, respectively, and ℓ_n are coefficients related to the Legendre polynomials [see Eq. (A11)]. The sign ambiguity in Eq. (8a) is resolved by the requirement that $|\alpha_0|>1$. Notice that to compute q_0^n , we need, in addition to the current value of ψ , all earlier values ψ_0^k which occur in the convolution on the right. This history is the price we must pay for having transparent boundary conditions. From Eq. (8) we construct the remaining e_j, q_j^n using the recursion relations of Eq. (7).

In like fashion, the transparent boundary condition on the right becomes $w_{j-1}^n=\alpha_jw_j^n+\beta_j^n$, with α_j, β_j^n given by [see Eq. (A17)]

$$\alpha_j=a_j\pm\sqrt{a_j^2-1}, \quad (9a)$$

$$\beta_j^n=d_j^*(a_j^*-\alpha_j)\psi_j^n+d_j(a_j-\alpha_j)\sum_{k=1}^n\ell_{n-k+1}\psi_j^k. \quad (9b)$$

Here d_j and a_j are the values of d_j and a_j , respectively, at the right boundary ($j=J$). Again, the correct root is that which makes $|\alpha_j| > 1$. Together with $w_j^n = e_{j-1} w_{j-1}^n + q_{j-1}^n$, Eq. (9) leads to the correct initial value for w_j^n ,

$$w_j^n = \frac{q_{j-1}^n + \beta_j^n e_{j-1}}{1 - \alpha_j e_{j-1}}, \quad (10)$$

from which we generate $w_{j-1}^n, w_{j-2}^n, \dots, w_0^n$ using $w_{j-1}^n = (w_j^n - q_{j-1}^n)/e_{j-1}$ as before. Finally, the wave function at the new time ψ_j^{n+1} is recovered from w_j^n by unfolding the previous transformations:

$$\psi_j^{n+1} = -\psi_j^n + i \frac{h^2}{3\Delta} \frac{\psi_j^n}{d_j} + \frac{w_j^n}{d_j}. \quad (11)$$

We close this section with three remarks concerning the use of transparent boundary conditions. First, transparent boundary conditions can be used with the Numerov scheme to improve accuracy at a modest computational cost. Equations (8) and (9) are written for the Numerov discretization of the Crank–Nicholson evolution problem. Without this refinement, the equations are identical but for the replacement $d=1$ in the final results, a small price to pay for improving the accuracy from $O(h^3)$ to $O(h^5)$. Second, because transparent boundary conditions require that we retain all past values of the wave function on the boundaries [to compute the convolution in Eqs. (8) and (9)], it is straightforward to reconstruct the solution for any previous time. In effect, the animation can be run backward, despite the apparent loss of information as the waveform moves beyond the field of view. For the same reason, however, the amount of information that must be stored and manipulated increases steadily with time, which brings us to the last point: the sharply increasing cost of evaluating the convolution in Eqs. (8) and (9) imposes a practical limit on the duration of the simulation. One strategy to deal with this problem consists of approximating the convolution kernel ℓ_n by a discrete sum of exponentials.¹¹ Sacrificing accuracy for speed in this way may be desirable in some applications, but will not be pursued further here.

In summary, the essence of the proposed algorithm for calculating time-dependent Schrödinger wave functions on a finite interval can be reduced to the following steps.

(1) Discretize the space and time variables as $x_j = x_0 + jh$ and $t_n = t_0 + n\Delta$. The spatial interval extends from x_0 to $x_0 + Jh$, corresponding to $0 \leq j \leq J$, and t_0 ($n=0$) denotes the initial time. In terms of the time step Δ and spatial grid size h , introduce new variables $g_j \equiv V_j - 2i/\Delta$, $d_j \equiv 1 - h^2 g_j/12$, $f_j^n \equiv 4i \psi_j^n/\Delta$, and $w_j^n \equiv d_j(\psi_j^{n+1} + \psi_j^n) - h^2 f_j^n/12$. Here $V_j \equiv V(x_j)$ and $\psi_j^n \equiv \psi(x_j, t_n)$ are the discrete versions of the system potential energy and wave function, respectively. Note that ψ_j^n is known from a previous step or from the initial waveform; with each new time step the problem is to find ψ_j^{n+1} or, effectively, w_j^n .

(2) Calculate e_j and q_j^n for $j=1, 2, \dots, J-1$ from their values at the left boundary $j=0$ and the recursion relations of Eq. (7). For transparent boundary conditions, the proper start values e_0 and q_0^n are given by Eq. (8) with $a_0=1 + h^2 g_0/2d_0$ and ℓ_n defined by Eq. (A11). The numbers e_j need be found only once at the outset, whereas the q_j^n must be recalculated at each time step.

(3) Use e_j and q_j^n to calculate w_j^n for $j=J-1, J-2, \dots, 0$ from the recursion relation $w_{j+1}^n = e_j w_j^n + q_j^n$ and the value of w_j^n at the right boundary $j=J$. For transparent boundary conditions, the boundary value w_j^n is given by Eq. (10) with the definitions Eq. (9) and $a_j = 1 + h^2 g_j/2d_j$.

(4) Recover ψ_j^{n+1} from w_j^n using Eq. (11).

III. IMPLEMENTATION AND RESULTS

We implemented the algorithm of the preceding section in Java to take advantage of Java's natural capabilities in the areas of Web integration and portability. These capabilities of Java must be balanced against its inferiority compared to C or FORTRAN for scientific programming. For example, Java has no native support for complex number arithmetic, an essential component of most scientific applications, including the one described here. Although third-party packages are available to fill the void, we constructed our own c-number class, limiting it to just the basic methods we require. Following Styer,¹² the complex-valued wave function is portrayed using a color-for-phase scheme, in which the phase is mapped to the hue (the degree of red, green, or blue) component of an hue-saturation-brightness color model. We also used GL4Java, an OpenGL package developed for the Java language that boosts graphics performance and allows for faster, smoother animations.¹³ Specific results are discussed below for several applications especially suited to transparent boundary conditions. The code used to generate these results is part of a larger package called QMTOOLS, which is available on request from the author and slated for inclusion with the 3rd edition of *Modern Physics* by Serway, Moses, and Moyer.¹⁴

A. Traveling Gaussian wave packet

The simplest nontrivial example of a time-dependent quantum wave function, the free Gaussian wave packet, has become a benchmark in numerical computations of this sort. The potential energy is everywhere zero for this case and the initial wave is described by

$$\psi(x, 0) = \exp(ikx) \exp(-[x - x_0]^2/2\sigma^2), \quad (12)$$

where σ determines the width of a packet centered at x_0 . We used $\sigma=0.125$ and $x_0=0.5$. The choice $k=50$ endows our packet with group velocity $2k=100$. The computational interval extends from $x=0$ to $x=1$, and includes a mere 160 points for a relatively coarse grid size of $h=1/160$. The packet has an observable amplitude over the approximate range $x_0 \pm 3\sigma$: at the end points, the amplitude $|\psi(0,0)| = |\psi(1,0)| = 3.35 \times 10^{-4}$, not zero as required by the theory, but small enough to have no appreciable effect. For the time step, we took $\Delta=10^{-5}$. As is well known, such a packet travels to the right and spreads uniformly, while retaining its Gaussian profile. Figure 1 shows our numerical results at $t=0.004$ and $t=0.009$. Notice the complete absence of any numerical reflections at the right boundary—clear evidence of transparent boundary conditions. For $t=0.009$, the packet is nearly absent from view; theory shows that at this time it is centered at $x=1.4$ and has spread to a width $\sigma = \sqrt{(0.125)^2 + 4(0.009)^2}/(0.125) = 0.191$, hence the “tail” still visible at the extreme right of Fig. 1(b).

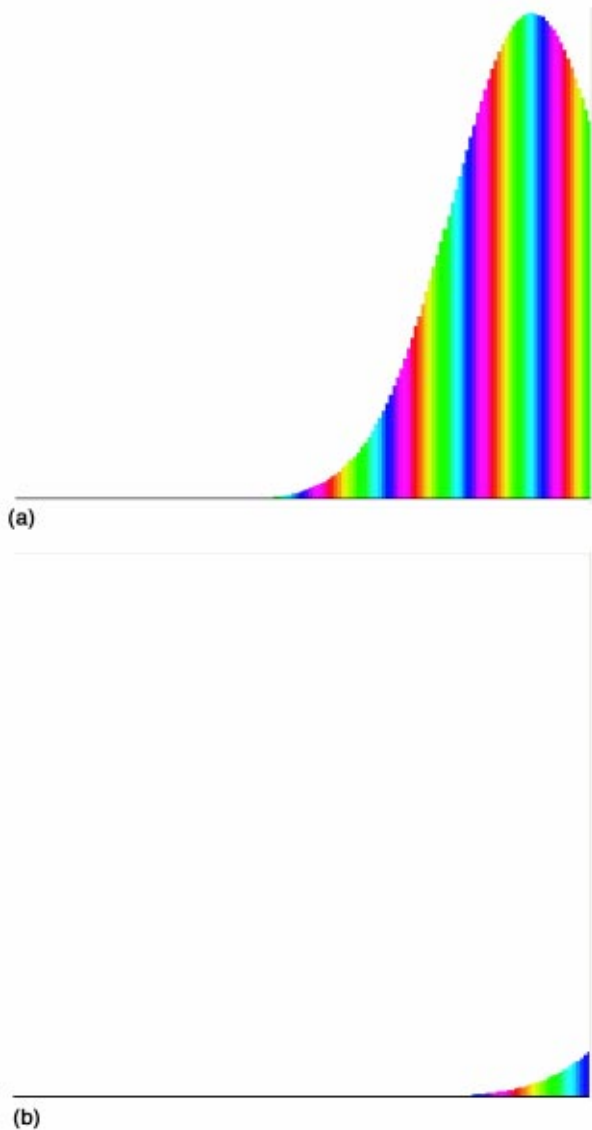


Fig. 1. A rightward-traveling Gaussian waveform $\psi(x,t)$ at (a) $t=0.004$ and (b) $t=0.009$. The interval shown is $0 \leq x \leq 1$. Shades of gray in black and white represent the phase of the wave. The complete absence of reflections at the boundaries results from the use of transparent boundary conditions. The initial waveform is given by Eq. (12) with $k=50$, $x_0=0.5$, and $\sigma=0.125$ in units where $\hbar=1$ and $m=1/2$.

B. Resonant scattering from a double barrier

Our next example is an application drawn from semiconductor device physics: a wave packet scattering resonantly from a double rectangular barrier. The initial wave is again Gaussian as in Eq. (12), but this time we used $k=0.31$, $\sigma=\sqrt{10}$, and $x_0=-25$ in units where length is measured in nanometers, time in femtoseconds ($1 \text{ fs}=10^{-15} \text{ s}$), and energy in electron volts. The barriers are 0.25 eV high and 5 nm wide, with a gap of the same width separating the two. For the particle mass we took $m=0.067m_e=34.24 \text{ keV}/c^2$. These choices model electron transport in a three-layer GaAs-Ga_{1-x}Al_xAs sandwich;¹⁵ the barrier regions are formed from the GaAs matrix by doping with about 30% Al content, and the effective mass of electrons in GaAs is about 0.067 of the free-electron value. The resulting heterostructure acts as a selective energy filter, transmitting only those

electrons with energies close to the eigenenergies of the potential well formed by the twin barriers. As it happens, the average energy of the incident wave packet, 0.083 eV, closely matches the ground state energy of this well. (In practice, the electron energy is fixed at the Fermi energy of GaAs, and the device is tuned to resonance by applying a suitable bias voltage that alters the well energies.)

The sequence shown in Fig. 2 illustrates the scattering event. The computational interval extends from -40 to $+40$ nm with a grid size $h=0.15625$ nm (512 points) and time step $\Delta=0.1$ fs. Figure 2(a) shows interference fringes developing on the leading edge of the incident wave as it first encounters the barrier, followed later by the emergence of a recognizable transmitted wave packet in Fig. 2(b). This transmitted wave is broader than usual, because it is composed of only those (relatively few) components in the incident packet with energies within the narrow range of resonance. The reflected wave in this case is unusual, being a multi-peaked, coherent wave train that moves with a speed that is independent of the average energy of the incident packet.^{16,17} Long after the main scattering event is over ($t=700$ fs), a small remnant of the initial wave remains trapped between the barriers, steadily losing amplitude with time [Fig. 2(c)]. This residual wave resembles the bound state at this energy and represents particle trapping; the accompanying time delay in the scattering process is a well-known consequence of resonance.

In the absence of transparent boundary conditions, this scattering event and subsequent particle trapping would be far more difficult to model effectively. With rigid-wall boundaries, we must be sure that the reflected and transmitted packets at the end of the event are out of the region of the potential, yet still far enough from the end points to avoid spurious reflections. The remedy adopted in Ref. 1 was to confine the event to the middle half of the interval, in effect “wasting” half of it. Given the initial packet speed ($\hbar k/m=0.541$ nm/fs), a very conservative estimate (which ignores wave packet spreading) places the rigid-wall interval length required to show Fig. 2(c) at about 760 nm, or nearly an order of magnitude larger than that for transparent boundary conditions. To preserve the same spatial resolution would require an increase in the number of grid points by the same factor.

C. Alpha decay of a radioactive nucleus

Our final example concerns radioactivity, and makes for an enlightening pedagogical activity. The potential is chosen to model alpha decay from a radioactive nucleus: it consists of a square well bounded on the right by a thin barrier (a “leaky” well). The well depth and barrier height are equal at 30 MeV and the width of the well and barrier are $L=5$ fm and $w=1$ fm, respectively. The mass is that of an alpha particle, $m=4.0026 \text{ u} \approx 3728 \text{ MeV}/c^2$ ($1 \text{ u}=931.5 \text{ MeV}/c^2$ is the atomic mass unit). The initial wave is a Gaussian confined to the potential well, to represent an alpha particle with its parent nucleus. For this example, we used Eq. (12) with $k=0$, $x_0=2.5$ fm (the midpoint of the well), and $\sigma=1.0$ fm, small enough to make the initial probability of finding the alpha outside the well negligible. The computational interval extends from $x=-3$ fm to $x=15$ fm and includes 512 points, for a grid spacing $h=3.5156 \times 10^{-24}$ fm. The time step is $\Delta=10^{-24}$ s.

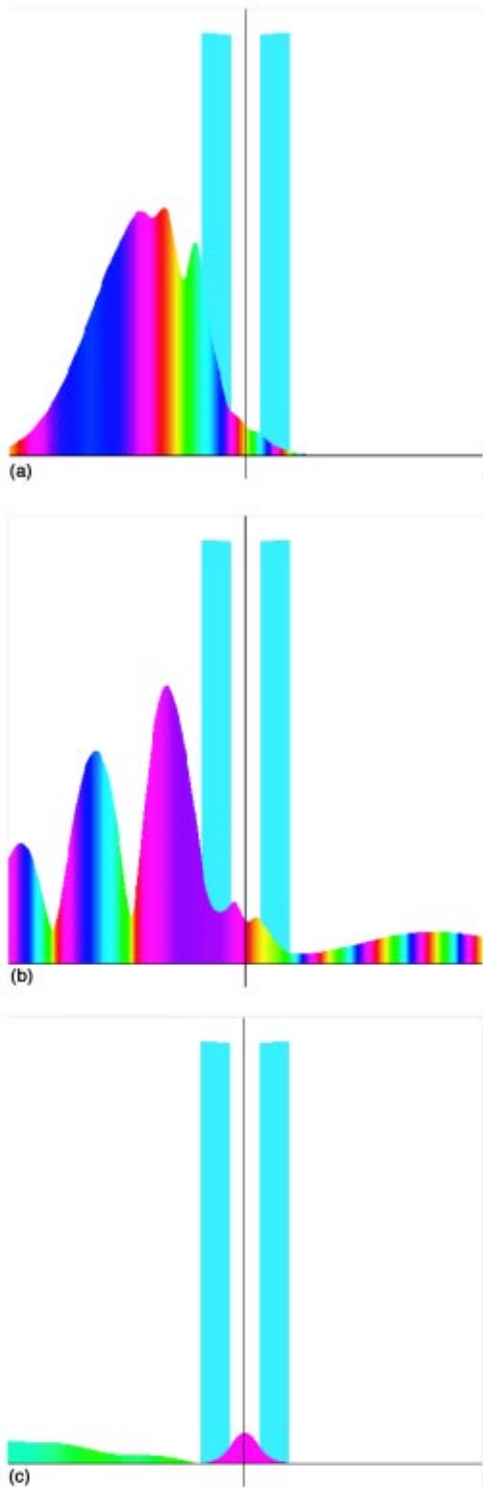


Fig. 2. Resonant scattering of a Gaussian wave packet $\psi(x,t)$ from a double barrier. (a) The incident packet first encounters the barrier at $t=16.0$ fs and (b) a recognizable transmitted wave emerges at $t=48.0$ fs. (c) Long after the encounter ($t=700$ fs), a remnant of the colliding packet remains trapped in the well formed by the two barriers. Parameters for the initial wave, Eq. (12), were chosen to model electron transport in a GaAs–Ga_{1-x}Al_xAs heterostructure, with the average packet energy, 0.083 eV, closely matching the lowest quasidiscrete energy of the well formed by the two barriers.

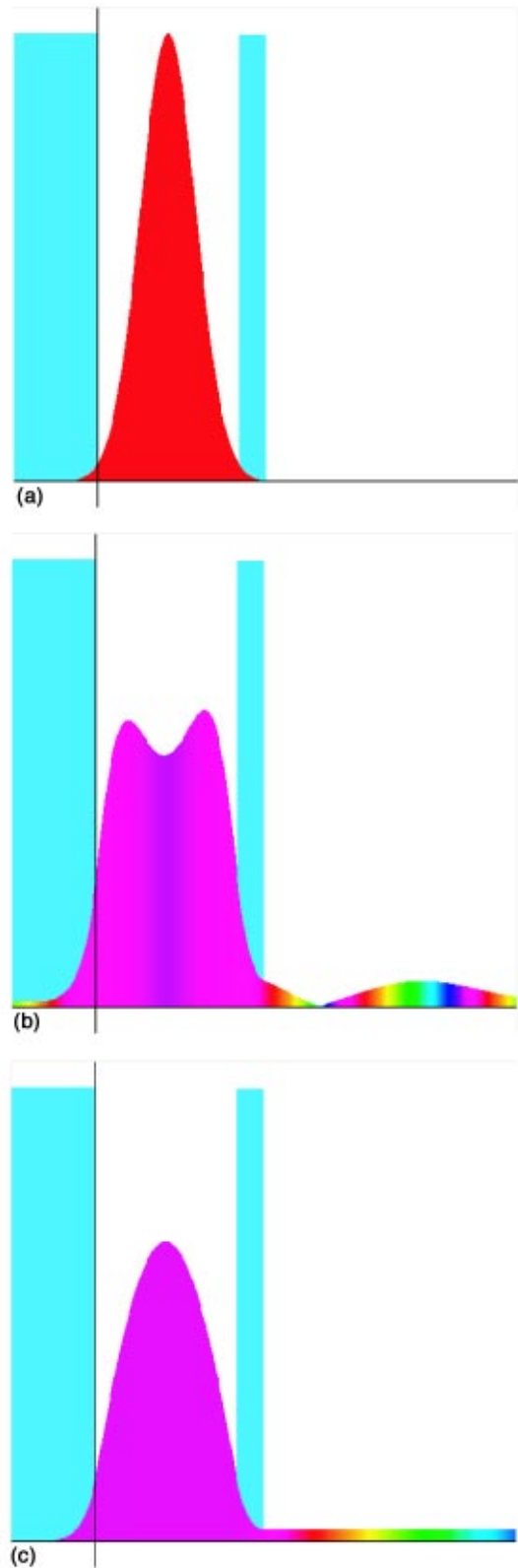


Fig. 3. Simulating alpha decay from a radioactive nucleus. (a) Initially the alpha is described by a Gaussian wave packet $\psi(x,t)$ localized to the nuclear well. (b) The short-term waveform “pulsates,” as shown for $t=0.0005$ as ($1 \text{ as}=10^{-18} \text{ s}$). (c) At $t=0.038$ as, the waveform has assumed a stable form marked by the steady flow of probability from the nuclear well. The average alpha particle energy is 2.622 MeV, well below the 30 MeV height of the nuclear barrier. The barrier thickness is 1 fm, and the interval shown extends from $x=-3$ fm to $x=15$ fm.

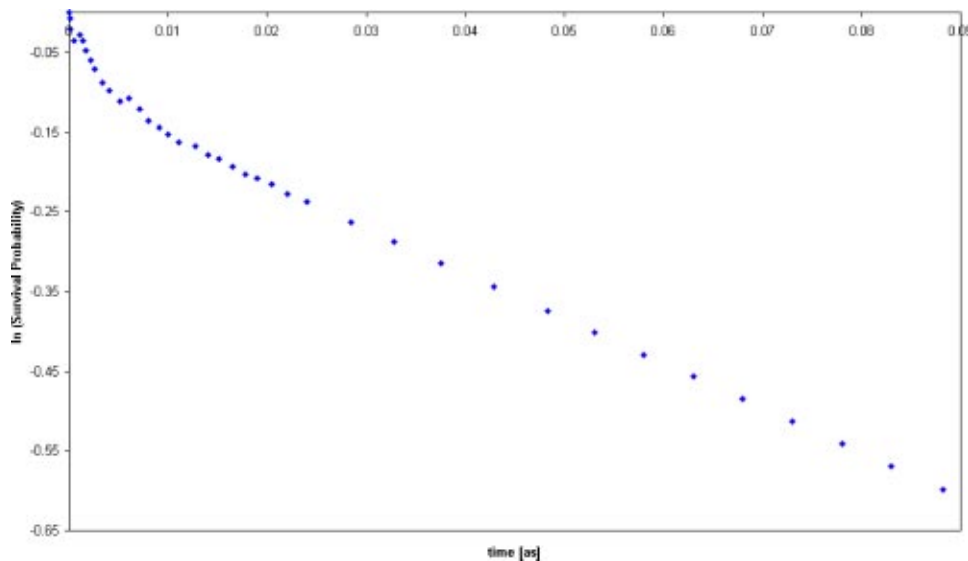


Fig. 4. The logarithm of survival probability vs time for the simulation of Fig. 3. The short-term fluctuations accompany the pulsating waveform shown in Fig. 3(b); these give way to the linear behavior that marks exponential decay for $t \geq 0.03$ as. A straight line fit to the data gives a decay rate $\lambda = 5.88 \times 10^{18}$ Hz, corresponding to a half-life of 1.18×10^{-19} s. The results agree within an order of magnitude with the predictions of the semiclassical model of radioactive decay.

Figure 3(a) shows the initial wave packet; at this instant, the alpha particle can be found in the well with probability 0.9996, or near certainty. The average alpha particle energy, 2.622 MeV in our model, is far below the height of the potential well (and somewhat above the lowest quasidecrete level energy, 1.508 MeV), so the alpha must tunnel through the barrier to escape. Figure 3(b) is illustrative of the waveform “pulsations” that characterize the early stages of decay. These pulsations gradually fade, eventually changing the original ψ to a form marked by a steady flow of probability from the nuclear well, as shown in Fig. 3(c).

As the simulation proceeds, we record the survival probability, the probability that the alpha particle can still be found within the confines of the potential well. Figure 4 shows the survival data at regular intervals plotted on a logarithmic scale. The abscissa is the time measured in attoseconds ($1 \text{ as} = 10^{-18} \text{ s}$). We observe clear short-term fluctuations that give way to a steady decline after about $t = 0.03$ as (some 30 000 time steps). The short-term fluctuations accompany the early pulsating waveform, while the linearity of the long-term data on a logarithmic scale implies exponential decay. The slope of this line, $5.88 \times 10^{18} \text{ s}^{-1}$, is the characteristic decay rate λ , from which we obtain the half-life $T_{1/2} = \ln 2 / \lambda = 1.18 \times 10^{-19} \text{ s}$ for this process. These results are to be compared with the standard semiclassical treatment which predicts exponential decay at a rate equal to the collision frequency multiplied by the barrier transparency at this energy. For (kinetic) energy $E = 2.622 \text{ MeV}$, the alpha has velocity $v/c = \sqrt{2(2.622)/3728} = 3.7505 \times 10^{-2}$, implying a collision frequency $f = v/2L = 1.124 \times 10^{21} \text{ Hz}$. And for alpha particles with $E = 2.622 \text{ MeV}$, the transmission factor for a square barrier 30 MeV high and 1 fm wide is readily found to be¹⁸ $T = 1.318 \times 10^{-2}$, giving a predicted decay rate $\lambda = fT(E) = 1.48 \times 10^{19} \text{ s}^{-1}$ and half-life $T_{1/2} = 4.68 \times 10^{-20} \text{ s}$. This order of magnitude agreement is likely all that we should expect from such a simplistic argument. As the simulation shows, the process of decay is far more complex than the semiclassical argument suggests (see, for example, the discussion by Kemble¹⁹). The same point has been emphasized again only recently, as analytical results reported for a semi-infinite well with a δ -function barrier show small, short-term fluctuations in the survival probability,

and the reappearance of oscillations in the long term which signal a crossover from exponential to power law behavior.²⁰ The former are reproduced in our simulation, but the latter are not, presumably because they occur at survival probabilities that are so small ($\sim 10^{-6}$ in the model calculations) as to require much too long to realize.

Again, transparent boundary conditions are indispensable to this application. With rigid-wall boundary conditions, decay from the nuclear well implies a buildup of probability in the adjacent well formed by the barrier and what is now an infinite barrier on the far right. In turn, this accumulation of probability leads to reverse tunneling, which interferes with the decay process under study. To determine a handle on this effect, we note that when the survival probability drops to 0.5, the reverse tunneling rate is simply the fraction L/L_0 of the forward amount, where L_0 is the width of the exterior well. To keep this undesirable effect at the 1% level would require a hundredfold enlargement of the computational interval, along with a proportionate increase in the number of grid points to maintain the same spatial resolution.

IV. CONCLUSION

The application of discrete transparent boundary conditions has been extended to include a Numerov discretization of the spatial grid. The improved accuracy afforded by this Numerov extension is shown to come at a modest computational cost. The method has been implemented in Java and demonstrated for two applications where the use of transparent boundary conditions is especially advantageous: simulating resonant scattering of electrons in a layered semiconductor, and modeling alpha decay from a radioactive nucleus.

ACKNOWLEDGMENTS

The author wishes to thank Professor Wolfgang Christian for directing him to the literature on transparent boundary conditions. Financial assistance for this project was provided through the generous support of the National Science Foundation under Grant No. DUE-9972322.

APPENDIX: TRANSPARENT BOUNDARY CONDITIONS IN THE NUMEROV APPROXIMATION

We outline the theory of discrete transparent boundary conditions when the Numerov approximation to the second derivative is used in the Crank–Nicholson evolution problem. The discussion extends the results presented recently by Ehrhardt.⁸

The equation to be studied is Eq. (6) with $w_j^n = d_j(\psi_j^{n+1} + \psi_j^n) - h^2 f_j^n/12$, $d_j = 1 - h^2 g_j/12$, $g_j = V_j - 2i/\Delta$, and $f_j^n = 4i\psi_j^n/\Delta$. The strategy is to solve Eq. (6) exactly in the exterior regions to obtain the proper connections at the left ($j=0$) and right ($j=J$) end points. In the exterior regions, we assume the initial waveform vanishes: $\psi_j^0 = 0$ for $j \leq 0$ and $j \geq J$. (In fact, the development also requires the initial wave to vanish at the neighboring points, $\psi_1^0 = \psi_{J-1}^0 = 0$.) The exterior regions also are assumed to be force-free, so that g_j and d_j become constants which we denote simply by g and d , respectively. It is also convenient to introduce $\lambda = 2h^2/\Delta$ (twice the parabolic mesh ratio).

Equation (6) is a difference relation in both the space (j) and time (n) indices. To handle the latter, we introduce the Z transform of ψ defined by

$$\tilde{\psi}_j(z) \equiv \sum_{n=0}^{\infty} \psi_j^n z^{-n}. \quad (\text{A1})$$

If we apply the Z transform to Eq. (6) in either exterior region, we find

$$\tilde{\psi}_{j+1}(z) + \tilde{\psi}_{j-1}(z) = 2a\tilde{\psi}_j(z) + i\frac{2\lambda}{d^2} \frac{1}{z+c} \tilde{\psi}_j(z), \quad (\text{A2})$$

with new constants $a = 1 + h^2 g/2d$ and $c = 1 - i\lambda/6d$. It is worth noting that $cd = d^*$, implying that c is a complex number of unit magnitude. The similarity to Eq. (6) suggests that we try the same method of solution, that is, introduce auxiliary functions $e_j(z)$ and $q_j(z)$ by requiring

$$\tilde{\psi}_{j+1}(z) = e_j(z)\tilde{\psi}_j(z) + q_j(z). \quad (\text{A3})$$

We substitute Eq. (A3) into Eq. (A2) and see that the auxiliary functions satisfy [see Eq. (7)]

$$e_j(z) + \frac{1}{e_{j-1}(z)} = 2a + i\frac{2\lambda}{d^2} \frac{1}{z+c}, \quad (\text{A4a})$$

$$q_j(z) = \frac{q_{j-1}(z)}{e_{j-1}(z)}. \quad (\text{A4b})$$

Because j does not appear on the right side of Eq. (A4), the recursion relation for $e_j(z)$ is satisfied by a uniform $e_j(z) = e(z)$, and Eq. (A4a) reduces to a quadratic form for $e(z)$. The two roots, say $e_{\pm}(z)$, are inverses: $e_+(z)e_-(z) = 1$. We use this last property to show that $q_j(z)$ can be made to vanish everywhere in the exterior region. On the left ($j = 0, -1, -2, \dots$), we choose the root $|e(z)| > 1$ to conclude from Eq. (A4b) that

$$q_j(z) = \frac{q_{j-1}(z)}{e(z)} = \frac{q_{j-2}(z)}{e^2(z)} = \dots = \frac{q_{j-N}(z)}{e^N(z)} \rightarrow 0. \quad (\text{A5})$$

Similarly, in the right exterior region we take the root $|e(z)| < 1$, to show $q_J(z) = q_{J+1}(z) = \dots = 0$. In this way, the

external problem in either region is reduced to

$$\tilde{\psi}_{j+1}(z) = e(z)\tilde{\psi}_j(z), \quad (\text{A6})$$

with $e(z)$ the proper root of Eq. (A4a). If we iterate Eq. (A6) a suitable number of times, we obtain $\tilde{\psi}_j(z)$ anywhere in the exterior in terms of its value at the end points, $\tilde{\psi}_{0,J}(z)$. However, inverting the Z transform of the result to recover ψ_j^n is a formidable task. Fortunately, the boundary conditions we seek require only that we invert Eq. (A6) where the interior and exterior regions meet, that is, at $j=0, J$. The inversion, while still challenging, is nonetheless doable.

We begin by writing an explicit result for the roots $e_{\pm}(z)$, which we recast in the following form:

$$(z+c)e_{\pm}(z) = az + a^*c \pm z\sqrt{a^2-1}\sqrt{1-2\mu x+x^2}, \quad (\text{A7})$$

$$\mu \equiv \frac{1-|a|^2}{|1-a^2|}, \quad (\text{A8})$$

$$x \equiv \frac{\exp(-i\phi)}{z}, \quad (\text{A9})$$

$$\phi \equiv \arg[(a^2-1)/c]. \quad (\text{A10})$$

The inversion of the Z transform requires a representation of the square root in inverse powers of z . The desired development follows directly from a Taylor expansion of $\sqrt{1-2\mu x+x^2}$ in powers of x , reminiscent of the generating function for Legendre polynomials. With some extra effort, we find

$$\sqrt{1-2\mu x+x^2} = -\sum_0^{\infty} \ell_n z^{-n}, \quad (\text{A11})$$

$$\ell_n \equiv \frac{\exp(-in\phi)}{2n-1} [P_n(\mu) - P_{n-2}(\mu)], \quad (\text{A12})$$

where P_n is the Legendre polynomial of degree n (negative subscripts imply a value of zero). Thus, $\ell_0 = -1$ and $\ell_1 = \mu \exp(-i\phi)$.

With these results, Eq. (A6) at the left boundary ($j=0$) becomes

$$(z+c)\tilde{\psi}_{j+1}(z) = \left[az + a^*c \mp z\sqrt{a^2-1} \sum_0^{\infty} \ell_n z^{-n} \right] \tilde{\psi}_0(z). \quad (\text{A13})$$

To invert the Z transform, we expand both sides of Eq. (A13) in powers of $1/z$ and equate coefficients of like powers. After some manipulation, we find the transparent boundary condition on the left

$$\psi_1^{n+1} + c\psi_1^n = (a \pm \sqrt{a^2-1})\psi_0^{n+1} + a^*c\psi_0^n \mp \sqrt{a^2-1} \sum_{k=1}^n \ell_{n-k+1} \psi_0^k, \quad (\text{A14})$$

or, in terms of the w_j^n ,

$$w_1^n = (a \pm \sqrt{a^2-1})w_0^n + (a^* - a \mp \sqrt{a^2-1})d^*\psi_0^n \mp d\sqrt{a^2-1} \sum_{k=1}^n \ell_{n-k+1} \psi_0^k. \quad (\text{A15})$$

Similarly, at the right boundary we take $j = J - 1$ in Eq. (A6) to obtain

$$\begin{aligned} \psi_{J-1}^{n+1} + c \psi_{J-1}^n &= (a \mp \sqrt{a^2 - 1}) \psi_J^{n+1} + a^* c \psi_J^n \\ &\pm \sqrt{a^2 - 1} \sum_{k=1}^n \ell_{n-k+1} \psi_J^k, \end{aligned} \quad (\text{A16})$$

or, equivalently,

$$\begin{aligned} w_{J-1}^n &= (a \mp \sqrt{a^2 - 1}) w_J^n + (a^* - a \pm \sqrt{a^2 - 1}) d^* \psi_J^n \\ &\pm d \sqrt{a^2 - 1} \sum_{k=1}^n \ell_{n-k+1} \psi_J^k. \end{aligned} \quad (\text{A17})$$

At each boundary, the relevant parameters a , c , and d (including μ and φ subsumed in the ℓ_n) take values appropriate to the adjoining exterior region, and these will differ if the left and right side saturation potentials V are not equal.

⁰Electronic mail: moyerc@uncwil.edu

¹A. Goldberg, H. M. Schey, and J. L. Schwartz, "Computer-generated motion pictures of one-dimensional quantum-mechanical transmission and reflection phenomena," *Am. J. Phys.* **35** (3), 177–186 (1967).

²Robert L. W. Chen, "Computer graphics for solutions of time-dependent Schrödinger equations," *Am. J. Phys.* **50** (10), 902–906 (1982).

³J. S. Papadakis, "Impedance formulation of the bottom boundary condition for the parabolic equation model in underwater acoustics," *NORDA Parabolic Equation Workshop*, NORDA Technical Note No. 143 (1982).

⁴B. Mayfield, "Non-local boundary conditions for the Schrödinger equation," Ph.D. thesis, University of Rhode Island, Providence, RI, 1989.

⁵V. A. Baskakov and A. V. Popov, "Implementation of transparent boundaries for numerical solution of the Schrödinger equation," *Wave Motion* **14**, 123–128 (1991).

⁶J. R. Hellums and W. R. Frensley, "Non-Markovian open-system boundary conditions for the time-dependent Schrödinger equation," *Phys. Rev. B* **49**, 2904–2906 (1994).

⁷A. Arnold, "Numerically absorbing boundary conditions for quantum evolution equations," *VLSI Design* **6**, 313–319 (1998).

⁸M. Ehrhardt, "Discrete transparent boundary conditions for general Schrödinger-type equations," *VLSI Design* **9**, 325–338 (1999).

⁹W. H. Press, B. P. Flannery, S. A. Teukolsky, and W. T. Vetterling, *Numerical Recipes* (Cambridge U.P., Cambridge, 1986), Sec. 17.2.

¹⁰It is even possible to have initial data that are supported outside of the computational domain, but the (considerable) numerical effort required in this approach is still open to investigation. See M. Ehrhardt, "Discrete artificial boundary conditions," Ph.D. thesis, Technische Universität Berlin, 2001.

¹¹A. Arnold, M. Ehrhardt, and I. Sofronov, "Discrete transparent boundary conditions for the Schrödinger equation: Fast calculation, approximation, and stability," preprint No. 753-2002, Institut für Mathematik, Technische Universität Berlin, 2002.

¹²J. R. Hiller, I. D. Johnston, and D. F. Styer, *Quantum Mechanics Simulations* (Wiley, New York, 1995).

¹³The GL4Java package and related documentation is available from www.jausoft.com/g14java.html.

¹⁴Raymond A. Serway, Clement J. Moses, and Curt A. Moyer, *Modern Physics* (Saunders College Publishing, Philadelphia, PA), 3rd ed., anticipated release date, March 2004.

¹⁵B. Mendez and F. Dominguez-Adame, "Numerical study of electron tunneling through heterostructures," *Am. J. Phys.* **62** (2), 143–147 (1994).

¹⁶A. P. Stamp and G. C. McIntosh, "A time-dependent study of resonant tunneling through a double barrier," *Am. J. Phys.* **64** (3), 264–276 (1996).

¹⁷G. Kalbermann, "Coherent polychotomous waves from an attractive well," *Phys. Rev. A* **60**, 2573–2576 (1999).

¹⁸The formula to compute $T(E)$ for a square barrier can be found in any elementary quantum physics text. See, for example, Raymond A. Serway, Clement J. Moses, and Curt A. Moyer, *Modern Physics* (Saunders College Publishing, Philadelphia, PA, 1997), 2nd ed., p. 231.

¹⁹E. C. Kemble, *The Fundamental Principles of Quantum Mechanics* (McGraw-Hill, New York, NY, 1937).

²⁰D. A. Dicus, W. W. Repko, R. F. Schwitters, and T. M. Tinsley, "Time development of a quasistationary state," *Phys. Rev. A* **65**, 032116 (2002).